Rectified Brownian motion and kinesin motion along microtubules

Ronald F. Fox and Mee Hyang Choi
School of Physics and Center for Nonlinear Science, Georgia Institute of Technology, Atlanta, Georgia 30080
(Received 16 May 2000; revised manuscript received 21 August 2000; published 6 April 2001)

The mechanism of rectified Brownian movement is used to analyze measured data for kinesin motion along microtubules. A key component of the mechanism is the diffusive movement of the microtubule binding heads of kinesin during the adenosine triphosphate (ATP) cycle. The first-passage time distribution for this step is analyzed in detail and is shown to be responsible for observed load-velocity profiles. The ATPase activity of the kinesin heads is that of a nucleotide switch and not that of a direct chemomechanical energy converter. Experimental data acquisition, rate constants, and alternative explanations are discussed. The mechanism described in this paper is fundamental to the nanobiology of intracellular processes.

DOI: 10.1103/PhysRevE.63.051901 PACS number(s): 87.16.Nn, 87.10.+e, 05.40.−a

I. INTRODUCTION

In an earlier paper [1], the mechanism of rectified Brownian movement was described and used to explain several chemomechanical energy conversions in molecular and cellular biology. The cases covered in that paper were ubiquinone transport across lipid membranes in electron transport chains, allosteric conformation changes in proteins, *P*-type ATPase ion transporters, several rotary arm enzyme complexes, and the dynamics of actin-myosin cross bridges in muscle fibers. The fundamental idea of rectified Brownian movement is that the metabolic free-energy currency of adenosine triphosphate (ATP) does no mechanical work directly, but instead is responsible for biasing boundary conditions for thermal diffusion. All work is done by thermal energy that is harnessed at the expense of metabolic free energy through the switching on and off of asymmetric boundary conditions. This idea, in various forms, has a long history in the literature [2,3].

In the present paper, this mechanism is used to analyze experimental data gathered on the behavior of kinesin as it moves along microtubules. Several kinds of data have been gathered. Rate constant data have been obtained and refined [4], new structural information has been elaborated very recently [5], and load-velocity profiles have been determined [6], most recently by means of improved optical tweezers techniques [7]. These data show that kinesin is capable of velocities as high as 1000 nanometers per second (nm/s) at low loads, decreasing to zero velocity with increased loads with a stall force of about 5–6 piconewtons (pN). In our model, this behavior is captured by the first-passage time distribution for the diffusive motion of a free kinesin head from one microtubule binding site to the next binding site.

A number of subtle issues arise with this analysis. These are addressed in this paper. In Sec. II, a biophysical description of the kinesin microtubule system is presented. In Sec. III, the basic steps of the ATP cycle are described. In Sec. IV, the rectified Brownian movement model is presented and analyzed. This analysis focuses on the first-passage time distribution function. Analytic and numerical results are presented. In Sec. V, problems with the measured load-velocity profiles and with reported rate constants are addressed. A discussion of alternative perspectives is given. These include Brownian ratchet mechanisms [8], a model invoking an ATP driven ''power stroke'' [9], and a model in which the load influences reaction rates directly [10].

The rectified Brownian movement model implies that the ATPase activity of the kinesin heads is that of a switch, like that of its ancestral protein, and not that of a direct chemomechanical energy converter.

II. PHYSICAL PROPERTIES OF KINESIN AND MICROTUBULES

Kinesins are a large class of ''motor'' proteins found in all organisms: protists, yeasts, plants, and animals. They fall within an evolutionary continuum starting with a primitive nucleotide switch, the putative ancester of *G* proteins, proceeding through kyosin, the motor precursor, and ending with parallel families of kinesins and families of myosins [5]. Kinesins are ATPases with two active ''heads'' that undergo an ATP activated attachment-detachment cycle coordinated by binding sites on microtubules. In this regard, they are similar to double-headed dyneins, which also travel along microtubules, and to double-headed myosins, which move along actin fibers. The attachment-detachment cycle requires one molecule of ATP [11] per head.

Microtubules are polymers of tubulin, a dimer of globular α-tubulin and β-tubulin subunits, each of which has a mass of 55 kilodaltons (kD). Microtubules undergo continuous assembly and disassembly at the expense of the energy in the γ-phosphate of guanosine triphosphate (GTP). The polymerized structure is a hollow cylinder of diameter 24 nm with the tubulin dimers oriented parallel to the axis of the cylinder. Electron microscopy and x-ray measurements suggest that microtubules consist of 13 axially parallel but staggered protofilaments. The protofilaments are made up of alternating head-to-tail linked α-tubulin and β-tubulin subunits. The α,β-dimers have a physical polarity and kinesin moves in one direction only, towards the ''plus'' end. There is one kinesin head binding site on each β-tubulin subunit of each tubulin dimer [5]. These sites are 8 nm apart along the axial direction. However, during the kinesin motion, each head moves from one binding site to the binding site two sites ahead, skipping the intervening site to which the other head is tightly bound (the width of a protofilament is 5.8 nm and

the width of a binding head is 4.5 nm). This process in then repeated by the other kinesin head while the original head remains tightly bound. Thus, in each step, a head moves a distance of 16 nm while the center of mass of the entire molecule moves only 8 nm. This is similar to the relative motions of our legs and our bodies as we walk. Indeed, it would be more natural to refer to the microtubule binding heads of kinesin as feet, but we will instead adopt the accepted terminology of heads.

Kinesin is a rather large molecule with a molecular weight around 500–600 kD. It is made up of two heavy chains and two light chains. The heavy chain contains the head, i.e., the motor unit, which is comprised of about 340–350 amino acid residues. This region has a rough size of $7.5\,\mathrm{nm}\times 4.5\,\mathrm{nm}\times 4.5\,\mathrm{nm}$. The head makes direct contact with the microtubule. The bulk of the heavy chain, called the ''neck'' [5], is a dimerized alpha-helical coiled coil. The total length of the complete kinesin is around 100 nm. The light chains are associated with the end of the molecule that binds the load. All of the catalytic activity is in the heavy chains. The ATP binding and hydrolysis takes place on the catalytic core of the heads. The neck is attached to the catalytic cores by segments of 15 amino acids called ''neck linkers'' [5]. The neck linker may be tightly docked to the core or simply adjacent to the core. These two states are dependent on which stage of the ATP cycle the kinesin head is in, as will be elucidated below.

III. KINESIN ATP CYCLE

The motion of kinesin along a microtubule is ''processive'' [11], i.e., many sequential steps occur before kinesin is completly released from the microtubule. ATP is essential during each cycle of head attachment-detachment [12]. At this point, we refrain from saying that ATP ''powers'' the cycle since our rectified Brownian movement mechanism clearly relies on heat to power the cycle, as we shall see.

The picture of how ATP hydrolysis is integrated into the whole process involves an alternating site (head) mechanism that has evolved with more detailed knowledge of the kinesin structure [4,5] and which differs from earlier models [9]. The cycle can be viewed as starting with a configuration in which the nucleotide-free leading head is tightly bound to the microtubule and the trailing head is unbound but has adenosine diphosphate (ADP) bound to it as a result of the previous cycle (see Figs. 1 and 2). The trailing head has just been released from the trailing head's microtubule binding site. ATP binds to the leading head and cannot bind to the trailing head because of its already bound ADP. The tightly bound leading head with its bound ATP remains bound to the microtubule while the unbound trailing head, at low load, rapidly diffuses to a new microtubule binding site, which is now further along the microtubule towards the plus end than is the site of the original leading head. Upon binding, it releases its ADP. Hydrolysis of the bound ATP, on what is now the new trailing head, ensues followed by *P* release and detachment of this ADP binding trailing head. This completes the cycle with the role of the two heads reversed. This coordination of ATP binding to one head and ADP release

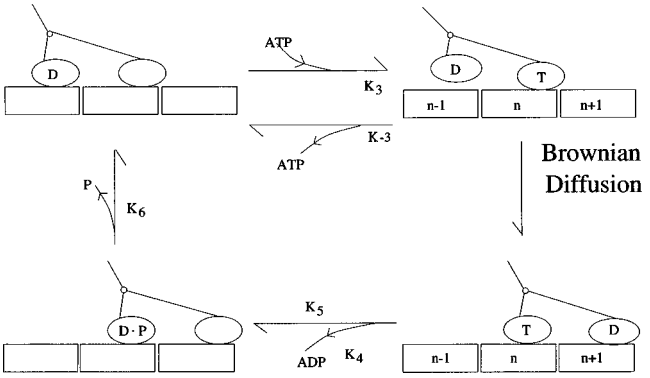

FIG. 1. This diagram presents the reaction scheme of Eq. (1). A portion of the microtubule is shown as a series of three rectangles, each of which represents an α-β dimer. The ovals represent the kinesin heads. The empty oval is tightly bound as is the ATP bound head that is depicted as an oval with a *T* inside. A head with ADP bound to it is weakly binding and is depicted with a *D* inside the oval. The oval with $D\cdot P$ inside it represents the state in which the head has bound ADP and *P* after hydrolysis of ATP. This causes the transition from strong to weak binding.

from the other head guarantees alternating ''steps'' by the heads. The neck linker is thought to play an important role in this process [5]. When ATP binds to the leading head, the neck linker becomes tightly docked to the catalytic core. Before docking, the neck linker of the leading head points backwards towards the neck that is between the two heads. The docking process attaches the neck linker to the core so that as the process proceeds with the trailing head executing Brownian movement until it finds its new binding site and becomes the new leading head, the neck linker is tightly docked facing forward to what is now the trailing head.

It has been suggested that ATP binding causes the forward motion of the neck linker and this in effect causes the unbound, ADP binding, trailing head to be ''thrown forward'' [5]. This is referred to as the ''power stroke'' [5]. However, here it is argued that the motion of the unbound

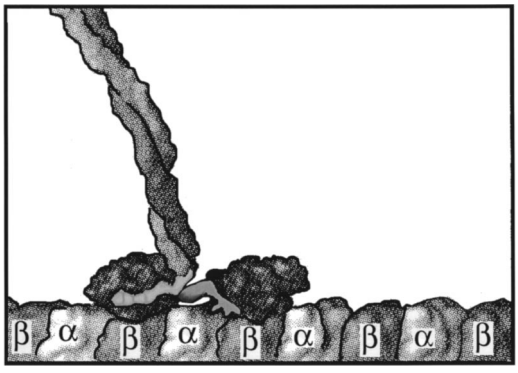

FIG. 2. The structure of kinesin attached to a microtubule. A piece of the neck and both heads are shown. The neck is a coiled coil and terminates in two neck linkers, one for each head. The neck linkers are depicted as light gray segments attached to the globular heads. The microtubule is shown as a single protofilament made up of alternating α-tubulin and β-tubulin. This figure is adapted from Ref. [5].

head from one microtubule binding site to another and the motion of the neck linker from the undocked position to the docked position is the result of Brownian diffusion. ATP binding and hydrolysis act as an irreversible switch to bias this Brownian movement. Thus the ATPase activity is similar to that of the evolutionary precursor switch protein [5].

The Langevin relaxation time is extremely short (on the order of picoseconds). For this reason, the process is really a diffusion process rather than a Langevin process [1]. This aspect of the process will be considered in detail in Sec. IV. An extremely short Langevin relaxation time means that the inertial term in the Langevin equation is negligible. A related way to express this is to say that the process is dominated by viscosity. Indeed, it occurs at very low Reynolds number ($<10^{-4}$). Thus the description of the process as involving the trailing head being ''thrown forward'' [5], or as ''akin to a judo expert throwing an opponent with a rearward-to-forward swing of the arm'' [5] is inapt since it would make sense only if the inertial term were important. In a more apt analogy, the judo expert would have to perform this maneuver while immersed in a large vat of molasses. In fact, this is also a poor analogy because the kinesin head motion is very random, i.e., the head executes rapid Brownian movement and does not simply move forward monotonically.

If elasticity of the kinesin protein is included, the final state of the rebound kinesin head may involve some elastic potential energy just after rebinding. The neck and its load subsequently relax with respect to this elastic strain very rapidly to a new temporary equilibrium. In the rectified Brownian movement model, this elastic energy is created by heat through the Brownian diffusion in accord with the Boltzmann distribution for potential energy. It is not created from the free energy contained in the γ-phosphate bond of ATP. If, on the other hand, one posits that the elastic energy is created by the ATP hydrolysis step, then it is said that a ''power stroke'' is involved in the mechanism [9]. In the rectified Brownian movement perspective, the free energy released during hydrolysis of ATP makes that step virtually irreversible and helps to switch on one of the boundary conditions for the thermal-diffusion process [1]. It does not generate elastic energy directly. This distinction regarding the significance of the hydrolysis of ATP is crucial in considering these models.

IV. RECTIFIED BROWNIAN MOVEMENT

The ATP cycle for a single kinesin head will be modeled in this paper in accord with the following chemical reaction scheme (see Fig. 1) [4,5]:

$$\mathrm{ADP}\cdot K+\mathrm{ATP}\underset{k_{-3}}{\overset{k_3}{\rightleftarrows}}\mathrm{ADP}\cdot K\cdot\mathrm{ATP}\Rightarrow\mathrm{ATP}\cdot K\cdot\mathrm{ADP}$$

$$\overset{k_5}{\rightarrow}\overset{k_4}{\rightarrow}\mathrm{ADP}\cdot\mathrm{P}\cdot K+\mathrm{ADP}\overset{k_6}{\rightarrow}\mathrm{P}+\mathrm{ADP}\cdot K. \tag{1}$$

In this scheme, $\mathrm{ADP}\cdot K$ denotes the leading kinesin head bound to a microtubulin binding site with ADP bound to the trailing head. The first step depicts the reversible binding of ATP to the leading head yielding kinesin with ATP bound to the leading head and with ADP bound to the trailing head, a state denoted by $\mathrm{ADP}\cdot K\cdot\mathrm{ATP}$. The double arrow depicts the Brownian diffusion step, which is irreversible for reasons to be elaborated below. It ends with the ATP bound head being the trailing head and with the ADP bound head weakly binding to a new microtubule binding site in the plus direction. This state is denoted by $\mathrm{ATP}\cdot K\cdot\mathrm{ADP}$. The third step is the virtually irreversible hydrolysis step that occurs while the new trailing kinesin head is still bound to the microtubule and while ADP is released from the new leading head, resulting in tight binding by the new leading head to the new microtubule binding site. These two steps occur on different heads and are parallel rather than sequential steps (this contrasts with Ref. [4], in which these steps are sequential). In the case of *P*-type ATPases [1], the analogous hydrolysis step results in the phosphorylation of an aspartate residue that retains most of the free energy of the γ-phosphate bond in ATP. Here, it is not known what the disposition of the *P* is. *P* is released from the trailing head causing the release of this ADP bound head from the microtubule and completing one ATP cycle. Each of these steps is virtually irreversible. Note that the ATP hydrolysis occurs after the heads change position so that it is extremely difficult to imagine how this energy could be involved in a ''power stroke.'' The indices chosen for the rate constants correspond to those used by Gilbert *et al.* [4] although the specific mechanism envisaged by them is not entirely identical with the more recent mechanism [5] which is adopted here (see above). If the *P* release rate constant quoted by Gilbert *et al.* [4] of 50 s^{-1} is taken as strict, then the maximum velocity possible for kinesin is less than 400 nm/s (*P* release is the rate-limiting step in the cycle and the center of mass moves 8 nm per step). This is much less than the observed velocity at high ATP concentrations.

The rate constant for ATP binding can be written as

$$k_3=[\mathrm{ATP}]k_3'. \tag{2}$$

At steady state, the first two steps of this process may be described by Michaelis-Menten kinetics [13]. This means that the reaction velocity $\overline{\nu}$ is given by

$$\overline{\nu}=V_{\max}\frac{[\mathrm{ATP}]}{[\mathrm{ATP}]+K_M}, \tag{3}$$

where $V_{\max}$ and K_M are defined by

$$V_{\max}=k_DK_T \quad \text{and} \quad K_M=\frac{k_{-3}+k_D}{k_3'} \tag{4}$$

and K_T is defined by

$$K_T=[K]+[K\cdot\mathrm{ATP}] \tag{5}$$

and k_D is defined as the reciprocal of the time taken for the diffusion step, *t*. If both the numerator and the denominator in Eq. (3) are multiplied by k_3' and Eq. (4) is used, then

$$\overline{\nu}=K_T\frac{k_Dk_3'[\mathrm{ATP}]}{k_3'[\mathrm{ATP}]+k_{-3}+k_D}. \tag{6}$$

This means that the effective rate for these two steps may be expressed as

$$\frac{k_D k_3'[\mathrm{ATP}]}{k_3'[\mathrm{ATP}]+k_{-3}+k_D}=\left(\frac{k_3'[\mathrm{ATP}]+k_{-3}+k_D}{k_D k_3'[\mathrm{ATP}]}\right)^{-1}=\left(\frac{1}{k_D}+\frac{1}{k_3'[\mathrm{ATP}]}+\frac{k_{-3}}{k_D k_3'[\mathrm{ATP}]}\right)^{-1}. \tag{7}$$

The total time it takes for the sequence of reactions and diffusion to occur as depicted in Eq. (1) is the sum of the reciprocals of the rates for each step with the exception of the parallel steps of hydrolysis and ADP release. For them, we need the time for the slower of the two parallel processes only. Since $k_4 > k_5$, the total time is given by

$$X_{\text{total time}}=\frac{1}{k_D}+\frac{1}{k_3'[\mathrm{ATP}]}+\frac{k_{-3}}{k_D k_3'[\mathrm{ATP}]}+\frac{1}{k_5}+\frac{1}{k_6}, \tag{8}$$

wherein $k_D=1/t$ as was noted above. The overall rate R for the entire process is the reciprocal of this total time.

Two points deserve emphasis at this stage of the argument. (i) Chemical reactions are stochastic processes too, so that the time for a reaction step is not simply the inverse of the reaction rate. This reaction rate is the mean reciprocal time. In the theory for the Arrhenius reaction rate formula [14], the distribution of reaction times is sharply peaked around a mean time so that no real error is introduced by ignoring this distribution altogether, as has been done here. (ii) The diffusion step has a distribution of times, called the first-passage time distribution, and as will be seen below, it is not sharp. On the contrary, it is quite broad so that the t implicit in Eq. (8) should be viewed as a single sample time and not as the mean time. Moreover, there is a significant difference between averaging Eq. (8) with respect to the distribution for t and then taking the reciprocal, and instead averaging the reciprocal expression for R, especially at high loads. Thus, the correct expression for the overall rate for the process in Eq. (1) is

$$\langle R\rangle=\left\langle\frac{[\mathrm{ATP}]k_3'k_5k_6}{[\mathrm{ATP}]k_3'(k_6+k_5+k_5k_6t)+k_5k_6+tk_{-3}k_5k_6}\right\rangle, \tag{9}$$

where $\langle\ \rangle$ denotes averaging with respect to the t distribution function. Velocities for kinesin moving along microtubules are given by $\langle R\rangle\times 8$ nm.

The determination of the first-passage time distribution for t occupies the bulk of this section, although the calculation itself is relegated to the Appendix. After the kinesin head detaches from the microtubule binding site, it engages in Brownian movement in accord with Langevin's equation,

$$M\frac{d\nu}{dt}=-6\pi\eta R_0\nu-f+\tilde{F}(t), \tag{10}$$

where ν is the velocity (this is the velocity for the kinesin head during the diffusion step and should be distinguished from the overall velocity of kinesin moving along microtubules given above), M is the mass of the head, R_0 is its radius (the ellipsoidal catalytic core head is approximated as a sphere), f is the load force, and $\tilde{F}(t)$ is a fluctuating force represented by Gaussian white noise with the properties

$$\langle\tilde{F}(t)\rangle=0,\quad\text{and}\quad\langle\tilde{F}(t)\tilde{F}(t')\rangle=2kT6\pi\eta R_0\delta(t-t'), \tag{11}$$

in which k is Boltzmann's constant and T is the temperature. The first term on the right-hand side of Eq. (10) is the Stokes drag appropriate for a sphere of radius R_0. From the physical dimensions of the kinesin head, $R_0=2.94$ nm, and the mass of the head is approximately $M=6\times10^{-20}$ g (350 amino acids averaging 110 D each). The aqueous medium of the cell around the kinesin head has a viscosity of approximately 0.01 poise (g/cm s). Therefore, $6\pi\eta R_0=5.54\times10^{-8}$ g/s and the Langevin relaxation time is

$$\frac{M}{6\pi\eta R_0}=1.08\times10^{-12}\ \text{s}, \tag{12}$$

which is so fast that the inertial term in Eq. (10) can be neglected. Thus, the effective description of the dynamics is given by the reduced version of Eq. (10),

$$\nu=-\frac{f}{6\pi\eta R_o}+\frac{\tilde{F}(t)}{6\pi\eta R_0}. \tag{13}$$

This is equivalent to the stochastic equation

$$\frac{dx}{dt}=-c+\tilde{g}(t), \tag{14}$$

where $c=f/6\pi\eta R_0$ and $\tilde{g}=\tilde{F}/6\pi\eta R_0$ with the properties

$$\langle\tilde{g}(t)\rangle=0\quad\text{and}\quad\langle\tilde{g}(t)\tilde{g}(t')\rangle=2kT\frac{1}{6\pi\eta R_0}\delta(t-t')=2D\delta(t-t'), \tag{15}$$

where Einstein's relation for the diffusion constant, D, has been used,

$$D=\frac{kT}{6\pi\eta R_0}=7.2\times10^{-7}\ \text{cm}^2/\text{s}. \tag{16}$$

This stochastic equation for x is equivalent to the diffusion equation [15], an example of a Fokker-Planck equation

$$\frac{\partial}{\partial t}P(x,t)=\frac{\partial}{\partial x}[cP(x,t)]+D\frac{\partial^2}{\partial x^2}P(x,t). \tag{17}$$

The boundary conditions are that the kinesin head starts at $x=a$, which is a reflecting boundary, and ends at $x=b$, which is an absorbing boundary. These boundary conditions exhibit the fact that once the ADP binding kinesin head detaches from its microtubule binding site, it is incapable of rebinding as a result of ADP induced conformational changes. It cannot go in the backward direction since the neck linker restrains it. When it reaches the new microtubule

binding site in the forward direction, it immediately binds, probably because its conformation in this new position is consistent with binding. This means that the flux vanishes at $x=a$, i.e. [14],

$$cP(a,t)+D\frac{\partial}{\partial x}P(a,t)=0 \quad \text{for all } t \tag{18}$$

and that P vanishes at $x=b$, i.e.,

$$P(b,t)=0 \quad \text{for all } t. \tag{19}$$

The initial condition is simply that

$$P(x,0)=\delta(x-a), \tag{20}$$

i.e., the kinesin head starts from the initial binding site.

In order to obtain the first-passage time distribution for this process, it is very convenient to use the backward equation [14]. Let $p(x_0,t|x)$ denote the distribution for the backward equation. It satisfies

$$\frac{\partial}{\partial t}p=-c\frac{\partial}{\partial x}p+D\frac{\partial^2}{\partial x^2}p \tag{21}$$

for $x\varepsilon[a,b]$ with the boundary conditions [14]

$$p(b,t)=0 \quad \text{and} \quad \frac{\partial}{\partial x}p(a,t)=0 \quad \text{for all } t \tag{22}$$

along with the initial condition

$$P(x_0,0|x)=\delta(x_0-x). \tag{23}$$

Note that the diffusion equation and the corresponding backward equation have different boundary conditions [14]. The probability that at time t the kinesin head is still in the interval $[a,b]$ is

$$\int_a^b dx' p(x',t|x)\equiv G(x,t). \tag{24}$$

$G(x,t)$ is the same as the probability that the time for reattachment, t_r, is greater than t [14]. From Eqs. (21)–(24) it follows that $G(x,t)$ satisfies

$$\frac{\partial}{\partial t}G=-c\frac{\partial}{\partial x}G+D\frac{\partial^2}{\partial x^2}G \tag{25}$$

with boundary conditions

$$G(b,t)=0 \quad \text{and} \quad \frac{\partial}{\partial x}G(a,t)=0 \quad \text{for all } t \tag{26}$$

and initial condition

$$G(x,0)=1. \tag{27}$$

There is an apparent inconsistency between the first condition in Eq. (26) and the condition in Eq. (27) at $x=b$ and $t=0$. This is illusory, having its origin in the nature of the Dirac δ function in Eq. (23). The completeness of the eigenfunctions for this problem will be used to express the δ function and the condition at $x=b$ will be clarified below. This detail is important in the numerical calculations that are described in Sec. V.

TABLE I. The mean first-passage time (MFPT) is given for different loads.

Load (pN)	MFPT (sec)
0	1.7727×10^{-6}
1	1.0991×10^{-5}
2	1.6465×10^{-4}
3	4.0071×10^{-3}
4	0.1231
5	4.3005
6	163.1
7	6541

If all that was needed was the mean first-passage time, $T(x)$, then this quantity could be obtained from $G(x,t)$ by [14]

$$T(x)=\int_0^\infty dt\, G(x,t). \tag{28}$$

It satisfies the differential equation

$$-c\frac{\partial}{\partial x}T(x)+D\frac{\partial^2}{\partial x^2}T(x)=-1 \tag{29}$$

subject to the boundary conditions

$$T(b)=0 \quad \text{and} \quad \frac{\partial}{\partial x}T(a)=0. \tag{30}$$

This problem has the closed-form analytic solution

$$T(a)=\frac{1}{c}\left\{\frac{D}{c}\left(\exp\left[\frac{c}{D}(b-1)\right]-1\right)-(b-a)\right\}. \tag{31}$$

For kinesin, $b-a=16$ nm. In the limit of no load, i.e., as $c\to0$, this expression simplifies to

$$T(a)\big|_{c=0}=\frac{(b-a)^2}{2D}=1.78\times10^{-6} \text{ s}. \tag{32}$$

This is very fast relative to the time scale for ATP binding, ATP hydrolysis, ADP release, and P release, each of which occurs in a time interval longer than a millisecond [2]. Table I shows how the mean first-passage time grows with load. While it is tempting to simply insert these numbers for t in the denominator of Eq. (9), it is not valid or accurate to do so because the first-passage time distribution is broad and it gets broader with increasing load. For example, when the load is 5 pN, given the values for the rate constants in Eq. (9) that will be introduced below, it is found that the value for $R\times8$ nm is 2.06 nm/s if the mean first-passage time of 4.3 s is inserted for t, whereas the value for $\langle R\rangle\times8$ nm is 10.9 nm/s if instead an average over the first-passage time distribution function is performed. This is a significant difference and requires that the first-passage time distribution be determined. Since this calculation is lengthy, it is relegated to the Appendix.

Figures 3(a)–3(c) show the first-passage time distribution for several different values of the load. As the load increases, the breadths of these distributions also increase, eventually

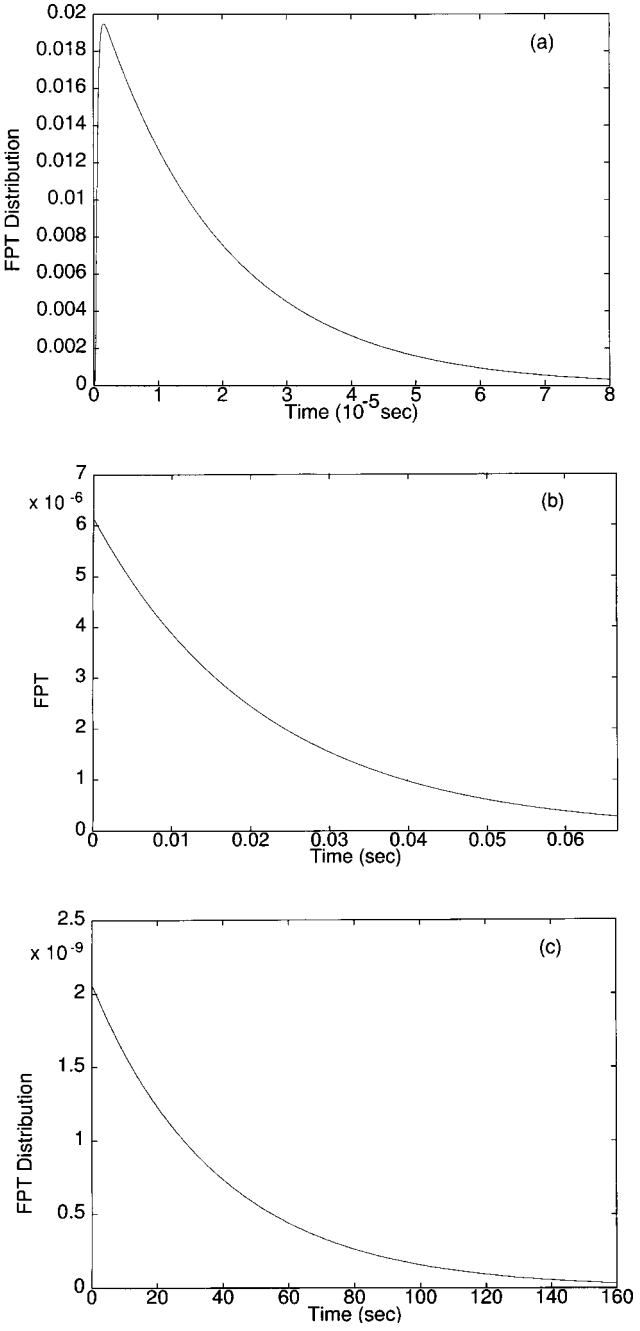

FIG. 3. (a) The first-passage time (FPT) distribution for a load of 1 pN is shown. The fact that it vanishes for very small t is visible. (b) The FPT distribution for a load of 3 pN is shown. On this time scale, the fact that the distribution vanishes for very small t cannot be seen. (c) The FPT distribution for a load of 5 pN is shown.

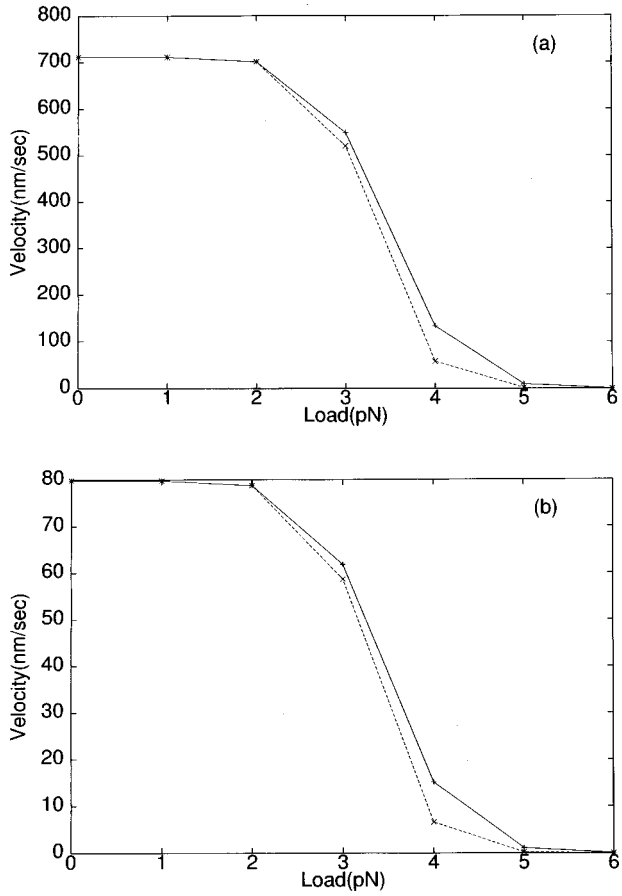

FIG. 4. (a) Load-velocity profile for $[\mathrm{ATP}]=2000\,\mu$M. The rate constants are those of Table II. The solid line is for averaging in accord with Eq. (9) whereas the dotted line is the result of simply replacing the t in the denominator of the right-hand side of Eq. (9) by $\langle t\rangle$. (b) Load-velocity profile for $[\mathrm{ATP}]=8\,\mu$M. The rate constants are those of Table II. The solid line is for averaging in accord with Eq. (9) whereas the dotted line is the result of simply replacing the t in the denominator of the right-hand side of Eq. (9) by $\langle t\rangle$.

covering several orders of magnitude. A quite good approximation to the first-passage time distribution for all loads is given by $(1/T)\exp[-t/T]$, in which T is the load-dependent mean first-passage time. The true first-passage time distribution vanishes for $t=0$ and then rises rapidly to the value given at $t=0$ by this approximation. This is evident in Fig. 3(a) but cannot be seen in Fig. 3(b) and 3(c) because of the compressed time axis. Table I shows how many orders of magnitude are covered as the load increases from 0 to 6 pN. In Figs. 4(a) and 4(b), it is shown how significant an error is made if instead of averaging over the first-passage time distribution in accord with Eq. (9), one instead simply places the mean first-passage time in the denominator in place of t. Clearly the latter approach results in a sharper cutoff and does not fit as well with the measured data, causing the stall force to be too small. To get these results, the rate constants Eq. (9) had to be changed from those quoted in Gilbert *et al.* [4] as is shown in Table II. In Figs. 5(a) and 5(b) [6] and 6 [7], data taken from the literature are reproduced. The salient points of comparison are as follows. (i) The rectified Brownian movement model predicts the same stall force as is found experimentally and gives the same maximum velocity at zero load, as a function of ATP concentration. While the rate constants are changed from the published [4] values, they do not differ by even an order of magnitude. (ii) The shape of the load-velocity curve for this model is a reverse sigmoid curve, whereas the experimental curves are quasilinear. This difference is pronounced at load lows because in the present model the velocity does not decrease noticeably until the

TABLE II. A comparison of chemical rate constants is given. Gilbert's constants are found in Ref. [4].

Rates	Description of rates	Gilbert's constants from Ref. [4]	Constants used to fit Refs. [6,7]	Constants used to fit Ref. [16]
k_3' ($\mu M^{-1}\,sec^{-1}$)	ATP binding per [ATP]	2	1.4	1.0
k_{-3} (sec^{-1})	ATP release	80	90	80
k_4 (sec^{-1})	ADP release	300	400	300
k_5 (sec^{-1})	hydrolysis	100	200	50
k_6 (sec^{-1})	phosphate release	50	170	30

load is 2–3 pN. This difference is discussed below.

Other recent data [16] have a profile closer to the sigmoid shape of the present calculations. These data are given in Figs. 7(a)–7(d). In Figs. 7(c) and 7(d), data are given for loads that are negative as well as positive. We are able to compare our results with the positive load portion of the data only. For negative loads, our model shows no increase in the velocity, as is seen in these figures. To do so would require explicit load-dependent reaction rate constants [10] that exhibit strain-induced changes in the rates [16]. While this is plausible, we have not yet found a good way to introduce this effect and, therefore, leave this aspect of the problem to future work. In Figs. 7(a) and 7(b) we show the results of our model for positive loads, but with rate constants that are modified relative to Gilbert's constants and relative to the modified constants already used above to compare with the other data. These constants are also given in Table II. While modifications of the rate constants are necessary to fit the data, the modifications are mild (not even an order of magnitude). What makes the data of Ref. [16] especially interesting from the perspective of this paper is that the velocity barely changes for loads up to 2 pN. This is consistent with our model and quite distinct from the results in Refs. [6,7].

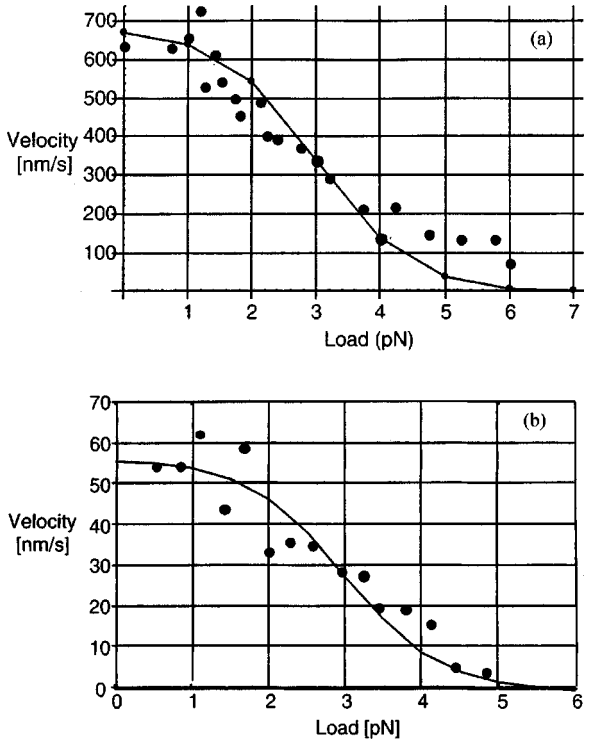

FIG. 5. (a) This load-velocity profile for $[ATP]=2000\,\mu M$ is redrawn from Peskin and Oster [9]. The solid curve is their reverse sigmoid fit to the data of Svoboda and Block [K. Svoboda and S. Block, Cell **77**, 773 (1994)] by the Peskin-Oster model. (b) This load-velocity profile for $[ATP]=10\,\mu M$ is redrawn from Peskin and Oster [9]. The solid curve is their reverse sigmoid fit to the data of Svoboda and Block [K. Svoboda and S. Block, Cell **77**, 773 (1994)] by the Peskin-Oster model.

V. DISCUSSION

Chemical assays used to determine the rate constants [4] are not the same as the experiments used to measure load-velocity curves. Thus, it should not be too surprising that there are mutual inconsistencies. The most glaring, referred to earlier in this paper, is that the quoted *P* release rate is 50 s^{-1} [4]. At 8 nm per ATP cycle, the center of mass of kinesin could only reach a velocity of at most 400 nm/s for this *P* release rate. Values approaching 1000 nm/s are observed. To make our results fit the load-velocity data [6,7], a *P* release rate of 170 s^{-1} was required. While Gilbert [17] does not insist on the slower rate, the higher rate used here is a bit outside the range Gilbert considers reasonable. The ADP release rate had to be 400 s^{-1} to obtain the results presented here, and the ATP dissociation constant had to be slightly increased as well (see Table II). The ATP binding constant used here is 1.4 $\mu M^{-1} s^{-1}$ as compared to the 2 $\mu M^{-1} s^{-1}$ used by Gilbert *et al.* [4]. Nevertheless, these adjustments of the rates are less severe than the corresponding disparity of rates used in earlier work [9].

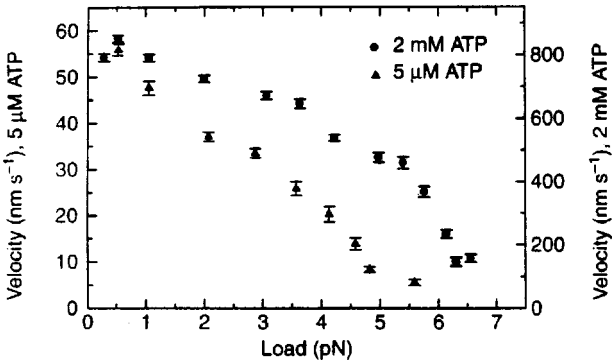

FIG. 6. These load-velocity profiles are redrawn from Visscher *et al.* [7].

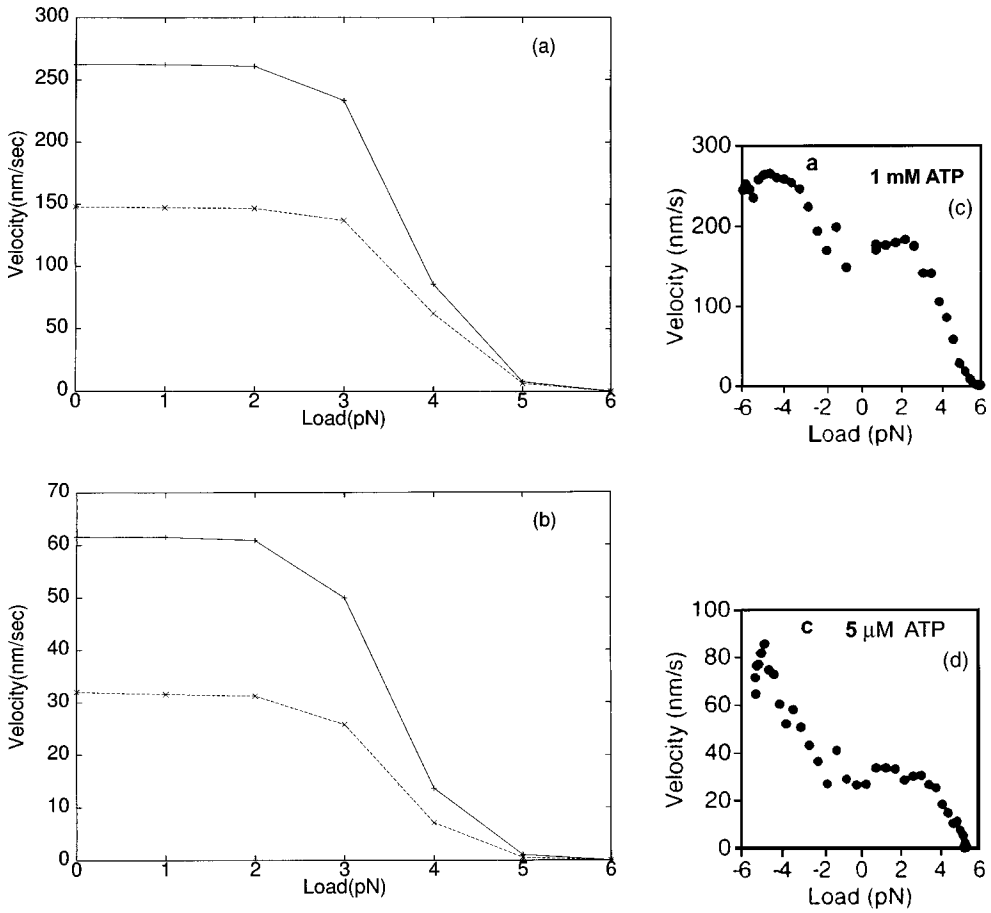

FIG. 7. (a) The load-velocity profile shown here is for 1 m*M* ATP. The solid curve is the result for rate constants given by Gilbert and listed in Table II. The dashed curve is for modified rate constants used to fit the data in Ref. [16]. (b) The load-velocity profile shown here is for 5 μM ATP. The solid curve is the result for rate constants given by Gilbert and listed in Table II. The dashed curve is for modified rate constants used to fit the data in Ref. [16]. (c) This figure is redrawn from Fig. 5(a) of Ref. [16]. The portion of the load-velocity profile for positive load only is to be compared with (a). (d) This figure is redrawn from Fig. 5(c) of Ref. [16]. The portion of the load-velocity profile for positive load only is to be compared with (b).

The key point of the work of Peskin and Oster [9] is that about 80% of the work done during one ATP cycle can be attributed to a ''power stroke'' whereas the remaining 20% is attributable to Brownian movement. While their model has many attractive features, it was constructed before the publication of the rate constants [4] and the new information on structure [5]. Thus, the detailed sequence of steps presented is no longer considered correct. Moreover, as mentioned earlier in this paper, it is possible to associate elastic strain energy with Brownian movement instead of with the energy released by the hydrolysis of ATP. If this is done, then the terminology of ''power stroke'' is no longer appropriate. For these reasons, the present model is not really in conflict with the Peskin-Oster model but rather represents an incorporation of newer information and a novel implementation of the idea of rectified Brownian movement through the first-passage time distribution that goes beyond their model.

A seemingly related mechanism is referred to as a thermal ratchet or as a Brownian ratchet. Such mechanisms have been comprehensively reviewed by Astumian [8]. They differ from the model of rectified Brownian movement proposed here in several important ways. Most significant is their dependence on a sawtooth potential and a lack of emphasis on boundary conditions for the diffusion process. To date, application of these models directly to a specific nanobiological system such as kinesin has not been made. However, the mechanism does work and nonbiological devices have been designed based on its principle of operation.

In another recent paper [10], a comprehensive account of motor protein mechanisms has been presented. In this paper, a minimal family of motor models is given in which the load appears directly in the rate constants, either for ''binding,'' for ''reaction,'' for ''release,'' or for ''triggering.'' The last case corresponds with the traditional power stroke point of view with chemical energy of ATP ''stored'' [10] in a strained state of the protein. While the model of rectified Brownian movement is clearly antithetical to this view, it nevertheless can be incorporated into the general scheme of Keller and Bustamante [10] by adding the kinesin head diffusion step to their reaction-rate sequence schemes. If this is done, then clearly there is load dependence explicitly in this diffusion step.

The apparent disparity between the shapes of the load-velocity curves determined by the rectified Brownian move-

ment model and by measurements may result from deficiencies in the model or from artifacts in the data, or both. Indeed, the difference between the reversed sigmoid shape for the load-velocity profile of the model and the quasilinear shape of some measured data [6,7] could lead some researchers to reject the model outright, although other data [16] do have the reversed sigmoid shape. That the model is potentially oversimplified is an easily accepted criticism. Its simplicity, however, is also one of its strengths since it provides a clear, intelligible foundation for understanding the overall process. To wit, the first-passage time distribution is the key to the load-velocity profiles. The measurements are likewise subject to criticisms. Two will be elaborated here.

The first criticism is based on the broad structure of the first-passage time distribution. This broad structure implies that sampling statistics will be important and in particular that larger sample sizes will be required as the load increases because the first-passage time distribution broadens greatly with this increase. In the measurements [6,7], the sample sizes are quite small, typically 10 to 100 samples per data point, often nearer the lower end of this range. Numerical simulations clearly demonstrate that such sample sizes are much too small for reliable statistics. This could partially explain why the data scatter at high loads is greater than the systematic error bars [6,7]. The numerical results presented in the preceding section were generated by numerical integration over the first-passage time distribution that was given analytically by the eigenfunction expansion. An alternative approach is to run stochastic simulations of the underlying stochastic dynamics given by Eqs. (14) and (15). While feasible for no load or for small loads, this approach is not feasible for loads on the order of 3–6 pN. The time taken for a single sample run becomes enormous and the number of runs needed for good statistics also becomes prohibitive as the load increases.

The second criticism is perhaps more significant. The measurements [6,7] were done using optical tweezers, a very elegant technique. This technique uses a feedback mechanism to position the silica bead, which is attached to the kinesin neck as the load, at a precise location in the optical tweezers. This location is chosen to correspond with a particular choice of load force. The tweezers are moved in response to the kinesin motion in order to maintain the bead at this location and thereby to maintain a constant load force. The bead position is sampled at 20 kilohertz (kHz) for this purpose. Needless to say, the actual applied force ''fluctuates'' around the desired constant load force as a result of this process [7]. In the paper of Visscher *et al.* [7], data for this effect are presented for an averaged constant load of 6.5 pN. The observed fluctuations in load are small and Gaussian. Nevertheless, they are fluctuations and they in effect create an additional fluctuating force operative during the diffusion process when the kinesin head moves from one microtubule binding site to the next. To estimate the magnitude of this effect, return to Eq. (11) and define the time-averaged fluctuating force

$$\tilde{f}=\frac{1}{\Delta t}\int_0^{\Delta t} dt\,\tilde{F}(t). \tag{33}$$

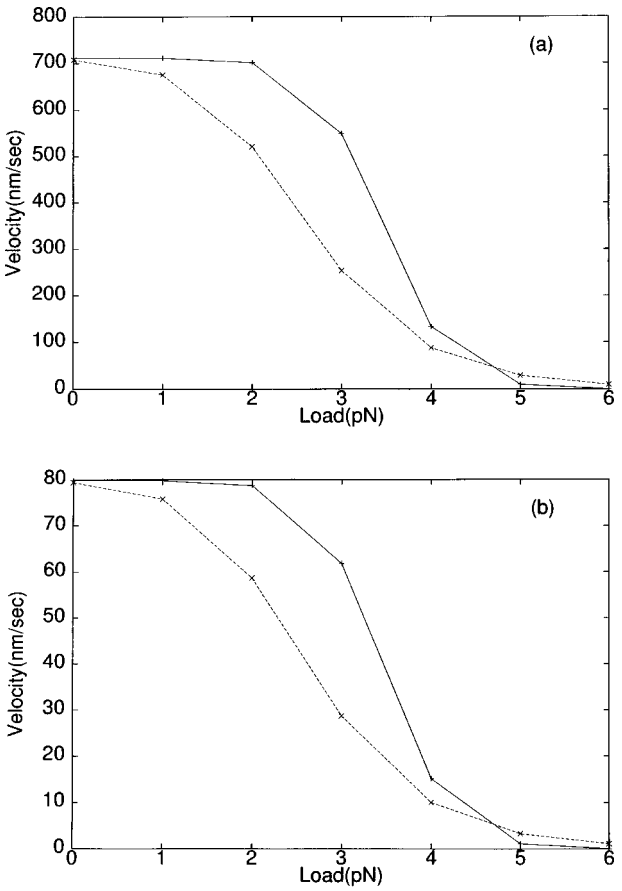

FIG. 8. (a) The load-velocity profile (dotted line) for [ATP] $=2000\,\mu$M with the enhanced D caused by the optical tweezers' noise and with a spring constant of $k_0=0.2$ pN/nm. The solid line is the solid line curve in Fig. 4(a). (b) The load-velocity profile (dotted line) for [ATP] $=8\,\mu$M with the enhanced D caused by the optical tweezer noise and with a spring constant $k_0=0.2$ pN/nm. The solid line is the solid line curve in Fig. 4(b).

Using the correlation formula in Eq. (11) implies that

$$\sqrt{\langle\tilde{f}^2\rangle}=\left(2kT\frac{6\pi\eta R}{\Delta t}\right)^{1/2}. \tag{34}$$

Incidentally, if $\Delta t=10^{-7}$ s is chosen in this formula, a time about one-tenth of the time required for diffusion of a load-free kinesin head from one microtubule binding site to the next, then the root-mean-square fluctuating force given by Eq. (34) is 2 pN. This shows just how robust the thermal forces are at the nanoscale. For a feedback sampling time corresponding to 20 kHz, i.e., $\Delta t=5\times10^{-5}$ s, the result is 0.089 pN. This is almost the magnitude of the applied force fluctuations for a mean force of 6.5 pN [7]. This means that in both Eq. (10) and Eq. (13) there should be a second, stochastically independent, fluctuating force added to $\tilde{F}(t)$. This implies that the D in Eq. (15) should be larger by about a factor of 1.5. The first-passage time distribution is quite sensitive to the value of D, as is the averaged rate $\langle R\rangle$. In Figs. 8(a) and 8(b) we show the load-velocity profile with D modified in this fashion. Elasticity of the neck linker has

been included with a spring constant, k_0, of 0.2 pN/nm. This means that Eq. (25) must be modified and takes the form

$$\frac{\partial}{\partial t}G = -(c+\overline{k}_0 x)\frac{\partial}{\partial x}G + D\frac{\partial^2}{\partial x^2}G, \tag{35}$$

in which

$$\overline{k}_0 = \frac{k_0}{6\pi\eta R_0}. \tag{36}$$

To get these results it was necessary to numerically integrate the equation for G since no analytic solution could be found. As mentioned earlier, care must be taken with the boundary condition at $x=b$. To check our procedure, direct numerical integration for G in the absence of elasticity was compared with the analytic results used above and very good agreement was observed. Since data for other mean applied force strengths were not published [7], a linear interpolation was used for loads different from 6.5 pN, starting from zero change in D at zero load and ending with $1.48\times D$ at a load of 6.5 pN, where D is the original value given in Eq. (16). These results suggest that the measured data potentially exhibit this effect since the agreement (the reversed sigmoid shape is substantially linearized) between the theoretical model and the data is improved noticeably by this artifice. It furthermore suggests that future use of the optical tweezers technique needs to take into account this systematic correction.

It has been shown that rectified Brownian movement provides a mechanism for kinesin motion along microtubules that is consistent with structural information [5], rate-constant measurements [4] and load-velocity profiles [6,7]. In the present model, the ATPase activity intrinsic to the kinesin heads acts as a switch rather than as a direct chemomechanical energy converter. The energy for motion comes from heat that is harnessed in a diffusion process involving asymmetric boundary conditions. The asymmetries are a consequence of ATP hydrolysis. The switch function is perhaps the same as that of the ancestral switch protein [5] that is also posited to be the ancester of G proteins that also act as switches. In G proteins, GTP is exchanged for bound guanosine diphosphate (GDP) [18]. This activates the G protein, which then usually activates adenylate cyclase (in some cases the effect is inhibitory rather than excitatory) until the GTP hydrolyses, thereby virtually irreversibly turning off the switch. ATPases functioning as switches rather than as direct chemomechanical energy converters have been proposed for a number of other mechanisms [19] in nanobiology, including mismatch repair in DNA. The switch interpretation is also applicable to the P-type ATPases described earlier [1]. Indeed, the switching activity is equivalent to allosteric nucleotide induction of a conformation change. In the rectified Brownian movement mechanism perspective of this paper, the switch function of the ancestral protein [5] is conserved in the modern descendants such as kinesin and myosin [1].

ACKNOWLEDGMENTS

This work was supported by National Science Foundation Grant No. PHY-9819646. The authors are grateful to Rick Fishel, Susan Gilbert, Charles Peskin, and Mark Schnitzer for helpful correspondence. Markus De Shon helped with the numerics and the figures.

APPENDIX

The backward equation with the boundary conditions and initial condition given by Eqs. (21)–(23) is solved efficiently by making the substitution

$$p(x,t) = U(x,t)\exp\left[\frac{c}{2D}(x-x_0) - \frac{c^2}{4D}t\right]. \tag{A1}$$

This implies the equation

$$\frac{\partial}{\partial t}U = D\frac{\partial^2}{\partial x^2}U \tag{A2}$$

with boundary conditions

$$U(b,t)=0 \quad \text{and} \quad \frac{\partial}{\partial x}U(a,t) + \frac{c}{2D}U(a,t) = 0 \quad \text{for all } t \tag{A3}$$

and initial condition

$$U(x,0) = \delta(x-x_0). \tag{A4}$$

Try solutions of the form $e^{-\lambda t}\cos(kx)$ and $e^{-\lambda t}\sin(kx)$. Therefore,

$$\lambda = Dk^2 \quad \text{or} \quad k = \pm\sqrt{\lambda/D}. \tag{A5}$$

A general solution has the form

$$U(x,t) = e^{-\lambda t}[A\cos(kx) + B\sin(kx)]. \tag{A6}$$

The boundary conditions require

$$A = -B\tan(kx) \quad \text{and} \quad A = B\frac{\frac{c}{2D}\tan(ka)+k}{k\tan(ka)-\frac{c}{2D}}. \tag{A7}$$

Therefore,

$$\frac{c}{2D}[\tan(kb)-\tan(ka)] = k[1+\tan(ka)\tan(kb)], \tag{A8}$$

which implies the eigenvalue equation

$$k = \frac{c}{2D}\tan[k(b-a)]. \tag{A9}$$

Introduce dimensionless $z = 2Dk/c$ and the eigenvalue equation becomes

$$z=\tan\left(z\frac{c}{2D}(b-a)\right). \tag{A10}$$

This equation, which is solved numerically, has countably infinitely many positive real roots except for the first, or lowest, root, which is real only if $c(b-a)/2D<1$. For $c(b-a)/2D\geqslant 1$, this root becomes purely imaginary (this transition occurs at a load of 0.5 pN). The solution in this case is

$$U=e^{\lambda t}[A\cosh(kx)+B\sinh(kx)] \tag{A11}$$

with the same relations as in Eq. (A5). The corresponding eigenvalue equation is

$$z=\tanh\left(z\frac{c}{2D}(b-a)\right), \tag{A12}$$

which has a single nontrivial solution only for $c(b-a)/2D\geqslant 1$. The trivial solution, $z=0$, implies $k=0$, which does not work since the boundary condition at $x=b$ cannot be satisfied except by the zero function.

Normalization follows from Eq. (A7) by writing

$$\begin{aligned}U_n(x)&=N_n[-\sin(k_nb)\cos(k_nx)+\cos(k_nb)\sin(k_nx)]\\&=N_n\sin[k_n(x-b)],\end{aligned} \tag{A13}$$

where the subscript n refers to the nth root of Eq. (A10). Forcing

$$\int_a^b dx\,U_n^2(x)=1 \tag{A14}$$

yields

$$N_n=\frac{1}{\left(\frac{1}{2}(b-a)-\frac{1}{4k_n}\sin[2k_n(b-a)]\right)^{1/2}}. \tag{A15}$$

Thus, for $c(b-a)/2D<1$,

$$U_n(x)=\frac{\sin[k_n(x-b)]}{\left(\frac{1}{2}(b-a)-\frac{1}{4k_n}\sin[2k_n(b-a)]\right)^{1/2}} \quad \text{for } n=0,1,2,\ldots. \tag{A16}$$

For $c(b-a)/2D>1$, the $n=0$ solution is instead

$$U_0(x)=\frac{\sinh[k_0(x-b)]}{\left(\frac{1}{4k_0}\sinh[2k_0(b-a)]-\frac{1}{2}(b-a)\right)^{1/2}}. \tag{A17}$$

Orthogonality follows from Eqs. (A2) and (A3) as follows:

$$\int_a^b dx\,U_n\left(U_{n'}''+\frac{c}{2D}U_{n'}'\right)=-\int_a^b dx\,U_{n'}'\left(U_n'+\frac{c}{2D}U_n\right), \tag{A18}$$

$$\int_a^b dx\,U_{n'}\left(U_n''+\frac{c}{2D}U_n'\right)=-\int_a^b dx\,U_n'\left(U_{n'}'+\frac{c}{2D}U_{n'}\right)$$

by integration by parts and because the boundary conditions kill the boundary terms at both $x=a$ and $x=b$. Subtracting the lower equation from the upper equation and rearranging terms yields

$$\int_a^b dx(U_nU_{n'}''-U_nU_n'')=0, \tag{A19}$$

which by Eqs. (A2) and (A6) implies

$$\left(\frac{\lambda_{n'}}{D}-\frac{\lambda_n}{D}\right)\int_a^b dx\,U_nU_{n'}=0. \tag{A20}$$

For $\lambda_n\neq\lambda_{n'}$, orthogonality follows.

We are now in a position to construct the solution to the backward equation [14]. It is

$$\begin{aligned}p(x_0,t|x,0)=\sum_{n=0}^{\infty}U_n(x_0)U_n(x)e^{-\lambda_nt}\\\times\exp\left[\frac{c}{2D}(x-x_0)-\frac{c^2}{4D}t\right].\end{aligned} \tag{A21}$$

The initial condition, Eq. (23), is satisfied because of the completeness of the eigenfunctions on the interval $[a,b]$ and at $x=b$ must vanish. Returning to Eq. (24) produces $G(x,t)$, which becomes

$$\begin{aligned}G(x,t)=\sum_{n=0}^{\infty}\left(1+\frac{4D}{c^2}\lambda_n\right)^{-1}U_n(x)\exp\left[-\lambda_nt-\frac{c^2}{4D}t\right]\\\times\left\{\frac{4D}{c}U_n(a)\exp\left[\frac{c}{2D}(x-a)\right]\right.\\\left.-\left(\frac{2D}{c}\right)^2U_n'(b)\exp\left[\frac{c}{2D}(x-b)\right]\right\}.\end{aligned} \tag{A22}$$

As a check, we can use Eq. (28) to obtain the mean first-passage time in the form

$$\begin{aligned}T(x)=\frac{c^2}{4D}\sum_{n=0}^{\infty}\left(1+\frac{4D}{c^2}\lambda_n\right)^{-2}U_n(x)\\\times\left\{\frac{4D}{c}U_n(a)\exp\left[\frac{c}{2D}(x-a)\right]\right.\\\left.-\left(\frac{2D}{c}\right)^2U_n'(b)\exp\left[\frac{c}{2D}(x-b)\right]\right\}.\end{aligned} \tag{A23}$$

This may not look much like Eq. (31) but it is identical and is the eigenfunction expansion of the quantity in Eq. (31). The expression in Eq. (A23) can be shown to explicitly satisfy Eq. (29) with the boundary conditions of Eq. (30).

[1] R. F. Fox, Phys. Rev. E **57**, 2177 (1998).
[2] A. F. Huxley, Prog. Biophys. Chem. **7**, 255 (1957); J. Physiol. (London) **243**, 1 (1974).
[3] T. Mitsui and H. Oshima, J. Muscle Res. Cell Motil. **9**, 248 (1988); M. Meister, S. R. Caplan, and H. C. Berg, Biophys. J. **55**, 905 (1989); R. D. Vale and F. Oosawa, Adv. Biophys. **26**, 97 (1990); N. Cordova, B. Ermentrout, and G. Oster, Proc. Natl. Acad. Sci. U.S.A. **89**, 339 (1991); S. Liebler and D. Huse, C. R. Acad. Sci. III **313**, 27 (1991).
[4] S. P. Gilbert, M. L. Moyer, and K. A. Johnson, Biochemistry **37**, 792 (1998); M. L. Moyer, S. P. Gilbert, and K. A. Johnson, *ibid.* **37**, 800 (1998).
[5] R. D. Vale and R. A. Milligan, Science **288**, 88 (2000).
[6] K. Svoboda and S. Block, Cell **77**, 773 (1994); K. Svoboda, P. P. Mitra, and S. M. Block, Proc. Natl. Acad. Sci. U.S.A. **91**, 11 782 (1994).
[7] K. Visscher, M. J. Schnitzer, and S. M. Block, Nature (London) **400**, 184 (1999); M. J. Schnitzer and S. M. Block, *ibid.* **388**, 386 (1997).
[8] R. D. Astumian, Science **276**, 917 (1997).
[9] C. S. Peskin and G. Oster, Biophys. J. **68**, 202s (1995).
[10] D. Keller and C. Bustamante, Biophys. J. **78**, 541 (2000).
[11] D. Voet and J. G. Voet, *Biochemistry* (Wiley, New York, 1995), p. 1024.
[12] W. Hua, E. C. Young, M. L. Fleming, and J. Gelles, Nature (London) **388**, 390 (1997).
[13] D. Voet and J. G. Voet, *Biochemistry* (Ref. [11]), pp. 351–353.
[14] C. W. Gardiner, *Handbook of Stochastic Methods* (Springer-Verlag, Berlin, 1983), Chap. 5.
[15] R. F. Fox, Phys. Rep. **48**, 179 (1978).
[16] C. M. Coppin, D. W. Pierce, L. Hsu, and R. D. Vale, Proc. Natl. Acad. Sci. USA **94**, 8539 (1997).
[17] S. P. Gilbert (private communication).
[18] D. Voet and J. G. Voet, *Biochemistry* (Ref. [11]), pp. 1276–1278.
[19] R. Fishel, Genes Dev. **12**, 2096 (1998); Nat. Med. **5**, 1239 (1999).